The International Journal of Advanced Manufacturing Technology (2025) 136:1267–1280
https://doi.org/10.1007/s00170-024-14927-4

ORIGINAL ARTICLE

Evaluating mixing methods for FFF-printed PLA-HA composites: Towards high-performance composites and advancements in additive manufacturing

Muhammad Zaryyab Sardar[1,2] · Kunal Manoj Gide[1] · Alexander Stuart[1] · Violetta Rostobaya[1] · Kian Zarrabinia[3] · Ali Beheshti[1] · Shaghayegh Bagheri[1]

Received: 11 September 2024 / Accepted: 9 December 2024 / Published online: 19 December 2024

Abstract
Additive manufacturing, particularly fused filament fabrication (FFF), enables the creation of polymer composites with precisely controlled mechanical properties. This control depends heavily on the mixing method during filament fabrication, which significantly impacts how reinforcing elements are distributed within the material. Despite its importance, a critical knowledge gap exists regarding how different mixing methods affect the mechanical properties of FFF-printed composites. This study evaluates three mixing methods—magnetic stirring (MS), wet speed mix (WSM), and dry speed mix (DSM) for polylactic acid-hydroxyapatite (PLA-HA) composites printed using the FFF method. The fabricated composites were assessed for mechanical properties using micro-indentation and isostatic compression tests, as well as topography and elemental composition via scanning electron microscopy (SEM) and energy-dispersive X-ray spectroscopy (EDS), respectively. Micro-indentation revealed the highest elastic modulus, indentation hardness, and creep resistance for DSM samples. Isostatic compression tests also corroborated these findings, with DSM leading to higher modulus of elasticity, modulus of resilience, absorbed plastic energy, and achievable compressive stress. EDS analysis confirmed the presence of HA particles within the PLA matrix for all three sample types. Among these three widely used mixing procedures, the findings of this study suggest that the DSM mixing method holds promise for fabricating high-performance FFF-printed polymer composites. While this study is limited to PLA-HA composites, the approach may offer a pathway for exploring its application to other ceramic-reinforced polymer composites in future research.

Keywords Fused filament fabrication · PLA-HA · Mixing methods · Mechanical properties · Surface and contact properties

1 Introduction

Additive manufacturing (AM) has revolutionized several industries by enabling the creation of complex objects with unparalleled design freedom [1–5]. Unlike traditional subtractive methods, AM builds objects layer-by-layer from a digital model, allowing for intricate geometries previously impossible to manufacture [3, 6]. This approach has led to the development of various AM techniques, each with its own strengths and materials [1, 3, 5–7]. Fused filament fabrication (FFF) is one of the popular and widely used AM techniques for polymers which operates by unwinding a filament, extruding it as a molten strand, and depositing it layer-by-layer onto a platform [8, 9]. Affordability, user-friendliness, and ability to rapidly produce intricate objects have made FFF ubiquitous across various industries [10–12]. However, while FFF printing offers advantages like lightweight construction and design flexibility, the mechanical strength or other properties like biocompatibility, chemical stability, and electrothermal properties, among others, often fall short for demanding applications [13–23]. This necessitates the development of methods to control and enhance these properties within FFF-printed objects. In particular, to address mechanical properties challenges, filler materials

✉ Shaghayegh Bagheri
sbagheri@gmu.edu

[1] Department of Mechanical Engineering, George Mason University, 4400 University Drive, Fairfax, VA 22030, USA

[2] Department of Chemistry and Biochemistry, George Mason University, 4400 University Drive, Fairfax, VA 22030, USA

[3] Northwest High School, 13501 Richter Farm Road, Germantown, MD 20874, USA

like carbon fibers, glass fibers, ceramics, or metallic particles have been utilized to be incorporated into the polymer matrix with significant enhancement in FFF-printed samples' mechanical properties [14, 16, 24–26].

The FFF technique offers profound potential in additively manufactured composites that can rival or even surpass traditionally manufactured parts [14, 27–35]. However, achieving optimal mechanical properties or for example, biocompatibility, in FFF composites also hinges on a crucial factor: the distribution of the filler material within the polymer matrix [5, 9, 36–40]. An uneven distribution can lead to weak interlayer bonding and the formation of voids or defects within the 3D-printed object [35–38, 41]. These imperfections act as stress concentrators, ultimately compromising the overall strength and performance of the composite [42–45]. Therefore, finding the optimum mixing methods employed during filament fabrication has become paramount [46–51].

In recent decades, hydroxyapatite (HA) has been incorporated into polymer composites to enhance their mechanical properties and biocompatibility [52–59]. Therefore, understanding the influence of different mixing methods on the mechanical properties of HA-reinforced composites has become crucial for unlocking their full potential and creating high-performance polymer composites for various applications [12, 52, 60–63]. PLA-HA (polylactic acid-hydroxyapatite) is one of the widely utilized composites that has been adopted for the FFF process. Previous studies showed that its mechanical properties and surface characteristics are highly influenced by mixing techniques. These properties ultimately determine their mechano-chemical suitability for mechanical and biomedical applications [28, 37, 42, 52–59]. However, existing research has primarily focused on optimizing the HA weight percentage within the PLA matrix using various mixing methods. For instance, Russias et al. [42] prepared PLA-HA composites of 50% and 90% by weight using methylene chloride as a saline coupling agent, while continuously mixing using the magnetic stirring (MS) mixing method. It was observed that composites with ceramic contents ranging between 70 and 85 wt% have higher mechanical properties but noted dissolution of the polymer matrix between the ceramic particles in the samples with higher HA w%. Corcione et al. [39] synthesized PLA-HA using the dry speed mix (DSM) method, where PLA and HA were pre-mixed using a rotomolding machine to produce PLA composite pellets where these pellets were subsequently processed to form a continuous filament suitable for feeding into a 3D printer. In their investigation, it was confirmed through scanning electron microscopy (SEM) and energy-dispersive X-ray spectroscopy (EDS) analyses that the HA content was homogeneously distributed within the PLA matrix in the composite filament. They also observed a slight increase in the flexural modulus compared to pure PLA. Petrovskaya et al. [64] took a comprehensive approach by synthesizing PLA-based composite materials with varying HA contents (0–30 wt%) using the MS mixing method. Their study optimized extrusion temperature, printing temperature, and printing speed for different mix proportions and delved into mechanical characterization through compression, flexural, and impact tests. Notably, PLA-HA composite with 30% HA content exhibited superior strength and endurance, surpassing the individual strengths of the constituents. Wu et al. [53] explored the application of the FFF process in 3D printing bone implants using 5, 10, and 15% HA-reinforced PLA polymer composites. Their approach involved a solution mixing process by the wet speed mix (WSM) technique, followed by molding into filaments using a single screw extruder. The study encompassed compositional, microstructural, and mechanical characterization. While the incorporation of HA enhanced mechanical properties, a trade-off with reduced print quality was observed. In another related study, Backes et al. [65] reported on improved thermomechanical properties in PLA-HA nanocomposites, observing enhanced cell proliferation at a 10% HA content. Their work synthesized nanocomposites through DSM technique and prepared FFF filaments, demonstrating the practicality of PLA-HA nanocomposites for AM applications with commendable print quality and accuracy. While these studies utilized various mixing methods to fabricate PLA-HA composites, none has directly compared the influence of mixing methods on mechanical properties and surface characteristics while keeping consistent final printing parameters, limiting our ability to predict and tailor the mechanical behavior of FFF composites based on the mixing method.

Current study utilizes FFF-printed PLA-HA composites as a model system to systematically compare three distinct mixing methods (MS, WSM, DSM), based on their efficacy in prior research [17, 26, 39, 42, 43, 66–69]. The primary objective of this study is to assess how various mixing methods impact the fabrication and mechanical properties of FFF-printed polymer-based composites, ensuring a thorough examination of their effects on mechanical performance while maintaining consistent final printing parameters. This work is novel in that it is the first study to directly compare the effects of different mixing methods on the properties of FFF-printed composites. We hypothesize that the properties of FFF-printed parts will be influenced by the pre-printing composite preparation, as the FFF process involves filament creation followed by layer-by-layer printing, which subjects the material to multiple cycles of heating and cooling. Additionally, the distribution of HA particles within the composite is qualitatively evaluated to better understand its effect on the mechanical properties. By investigating the influence of various mixing methods on PLA-HA composites in FFF printing, this study aims to contribute to the development of advanced, biocompatible materials for additive manufacturing applications. In what follows, methodologies for the

three mixing methods, sample preparation, printing parameters, micro-indentation testing, SEM/EDS, and compression tests are outlined in Section 2. Following this, Section 3 presents the results of these tests, alongside comprehensive one-way ANOVA analysis. Subsequently, in Section 4, a detailed discussion of the results is provided, drawing comparisons with previous studies to contextualize the findings. Finally, Section 5 encapsulates the conclusions drawn from the research findings, highlighting key insights and potential implications for future studies in the field.

2 Materials and methods

2.1 Materials and equipment

PLA was purchased from IC3D Printers (Dublin, OH, USA) while HA powder was acquired from Sigma-Aldrich (St. Louis, MO, USA). The MS mixing process was performed using C-MAG HS 10 MS apparatus (Fisher Scientific, USA) while DAC 150.1 FVZ-K speed mixer (Hauschild, Germany) was utilized for the DSM and WSM processes.

2.2 Mixing methods

2.2.1 Magnetic stirring (MS)

Here, the method proposed by Russias et al. [42] was selected to prepare PLA-HA composite using a magnetic stirrer, which has been shown to create strong interfacial adhesion and a homogeneous slurry suitable for FFF printing. 19.8 grams of PLA pellets were combined with 80 ml of dichloromethane (DCM) (Sigma-Aldrich, St. Louis, MO, USA) to first liquefy the solid PLA with a magnetic stirring apparatus, which includes a rotating magnetic bar, and a hot plate set at 25 °C for 4 h. After 4 h, when the PLA pellets had completely dissolved, 0.2 g of HA and 5 ml of WD-10 were added. This solution was then stirred at 25 °C at the slowest speed using the same magnetic stirring apparatus until uniform, resulting in 1 wt% of PLA-HA composites. It was then transferred to an aluminum tray to air dry and solidify into a thin sheet overnight.

2.2.2 Wet speed mix (WSM)

A "wet composite process" implemented by Zhang et al. [43] was used to fabricate the PLA-HA composite to achieve blending between the PLA and HA components. Due to the limited capacity of the speed mixer, the WSM process utilized half the usual quantities of ingredients. Two batches were prepared, each containing 40 ml of DCM, 9.9 g of PLA pellets, 0.1 g of HA, and 2.5 ml of WD-10. First, the PLA pellets were completely dissolved in the DCM using the magnetic stirring apparatus similar to what was mentioned in Section 2.2.1. Then, the HA was added to each batch of the PLA solution in the speed mixer. Each batch underwent two mixing cycles at 3000 rpm for 15 s each. The mixtures from both batches were then combined and transferred to an aluminum tray. The combined mixture was air-dried overnight in the tray, solidifying into a thin sheet.

2.2.3 Dry speed mix (DSM)

Here, we implemented a method used by Backes et al. [65] to prepare PLA-HA composite, as this method has demonstrated a good dispersion of HA particles, and satisfactory printing quality [65]. Unlike WSM that involved solvents or liquids, this technique operated entirely in a dry state which provided a rapid approach to effectively blend PLA and HA. Two batches were prepared, each containing 9.9 g of PLA pellets and 0.1 g of HA. Each batch underwent two cycles at 60 rpm for 5 min to achieve thorough mixing before the extrusion process began.

2.3 Filament extrusion

The dried sheet of PLA-HA from all three methods was cut into shreds not exceeding 6 mm in length, and subsequently, filament extrusion was conducted using a filament extruder (Noztek Pro HT, West Sussex, England) set to temperatures ranging from 180 to 210 °C. To prevent moisture absorption, the extruded filaments were stored in a plastic vacuum seal bag before printing.

2.4 Sample preparation

The sample was digitally designed with dimensions of 25.4 mm in length, 12.7 mm in width, and 12.7 mm in height using Autodesk AutoCAD 24.3 (San Francisco, USA). The dimensions complied with the ASTM D6264 standard [70] for the micro-indentation tests. The design file was then converted into G-code using Ultimaker Cura 5.7.0 (Zaltbommel, Netherlands) slicing software. The FFF printing process was carried out using the CreatBot F160 printer 3DPO-344 (Henan Province, China) at an ambient temperature of 23 °C. The samples were printed with a constant rectilinear infill pattern to ensure consistency across the mixing methods. To maximize adhesion to the build plate and minimize warping, the largest surface area of the sample was oriented horizontally during the FFF printing. All printing parameters are outlined in Table 1.

2.5 Polishing

To maintain uniformity in the indentation tests, the surfaces of all samples underwent manual polishing to achieve

Table 1 FFF printing parameters

Infill density (%)	Infill pattern	Build plate adhesion	Nozzle temperature (°C)	Bed temperature (°C)	Layer height (mm)	Print speed (mm s^{-1})
70	Lines	None	210	50	0.1 mm	200

a smooth finish. The polishing procedure involved a successive use of 600, 800, 1200, 2500, 3000, and 4000 grit electro-abrasive sanding papers, each for 5 min, employing both vertical and horizontal motions. A circling motion was then applied to ensure surface evenness. Figure 1a and b shows SEM images of the sample surfaces before and after polishing. The white arrows in Fig. 1 indicate the roughness lines on the surface of the sample. Following polishing, the surfaces were cleaned with 99% isopropyl alcohol to remove any residual polishing debris or contaminants.

2.6 Micro-indentation test

Micro-indentation tests were conducted using Anton Paar MicroCombi machine (Graz, Austria) equipped with a micro-vickers tip. Tests were performed with a loading/unloading rate of 1000 mN min^{-1} and at a maximum load of 300 mN under ambient conditions to obtain force vs. displacement curves. To ensure accuracy, four indentations were made on each sample in a 2 × 2 matrix spaced 200 µm apart where elastic modulus and indentation hardness were determined [71]. Creep analysis was also conducted separately to assess time-dependent deformation in PLA-HA composite. Indentations for creep experiments consisted of loading to a maximum load of 300 mN, holding the load constant at 300 mN for 100 s (creep loading) and then unloading to zero load. Utilizing displacement vs. time curves, the graph was analyzed during the 100-s pause. The difference between the final (h_f) and initial indentation depths (h_i) was used to measure material creep deformation (indentation creep Δh), following the techniques described in [72, 73].

2.7 SEM and EDS analyses

To examine various surface images, a Jeol JSM-7200F Field Emission Scanning Electron Microscope (Musashino, Akishima, Tokyo) was utilized to observe the sample surface layers both before and after polishing and capture the surface of post-compression (failed) samples. Elemental composition analyses were performed on the filament of each sample using EDS (Ametek-Gatan, USA) system. Given that the analyzed samples and their respective filaments were non-conductive polymers, a vacuum sputter coater (Denton, USA) was employed to apply a gold coating over the sample surface. One sample along with its filament from each mixing method was positioned inside the chamber, where pure argon gas was used to create an inert environment. For SEM imaging, three sets of machine parameters were utilized: a voltage of 1.5 kV and a probe current of 13 mA with a magnification of × 30 were used to capture the surface morphology. A 100 µm × 100 µm region on filaments from

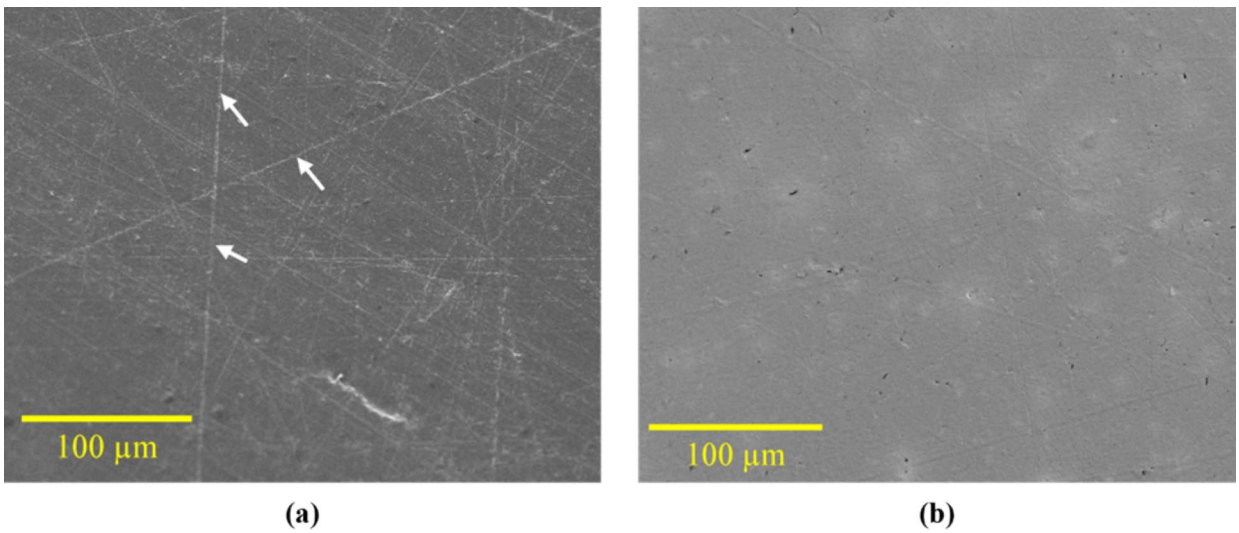

Fig. 1 SEM images (× 100 magnification) of the indentation sample's surface (**a**) before and (**b**) after polishing

each mixing method was selected for SEM imaging and subsequent EDS analysis to assess elemental variations. In addition, to evaluate the phosphorous-to-carbon (P/C) ratio distribution, a random 30-point EDS analysis was also conducted within this region, as shown in Fig. 2 to qualitatively assess the HA particle distribution and its influence on the mechanical properties. All EDS analyses were performed at 3.5 kV, with a probe current of 15 mA.

2.8 Compression test

To assess the compressive properties, compression tests were conducted on samples using Instron's Universal Testing Machine 5980 (±250 kN) Series (Instron, USA). Samples were securely positioned in the center of grips and compressed at a rate of 1.3 mm min^{-1} until a strain displacement of 50% was reached. All tests were conducted in accordance with the ASTM D695-15 standard [74] and were carried out at ambient temperature. The elastic region of the stress–strain curve was used to calculate the modulus of elasticity while compressive yield strength was determined using the 0.2% offset criterion. The area under the curve within the elastic region was used to quantify the modulus of resilience where absorbed plastic energy until 50% strain ($APE_{50\%}$) was obtained by calculating the total area under the plastic stress–strain curve up to 50% strain. Finally, the maximum achievable compressive stress up to 50% strain ($MACS_{50\%}$) was identified as the maximum stress the sample withstood up to 50% strain.

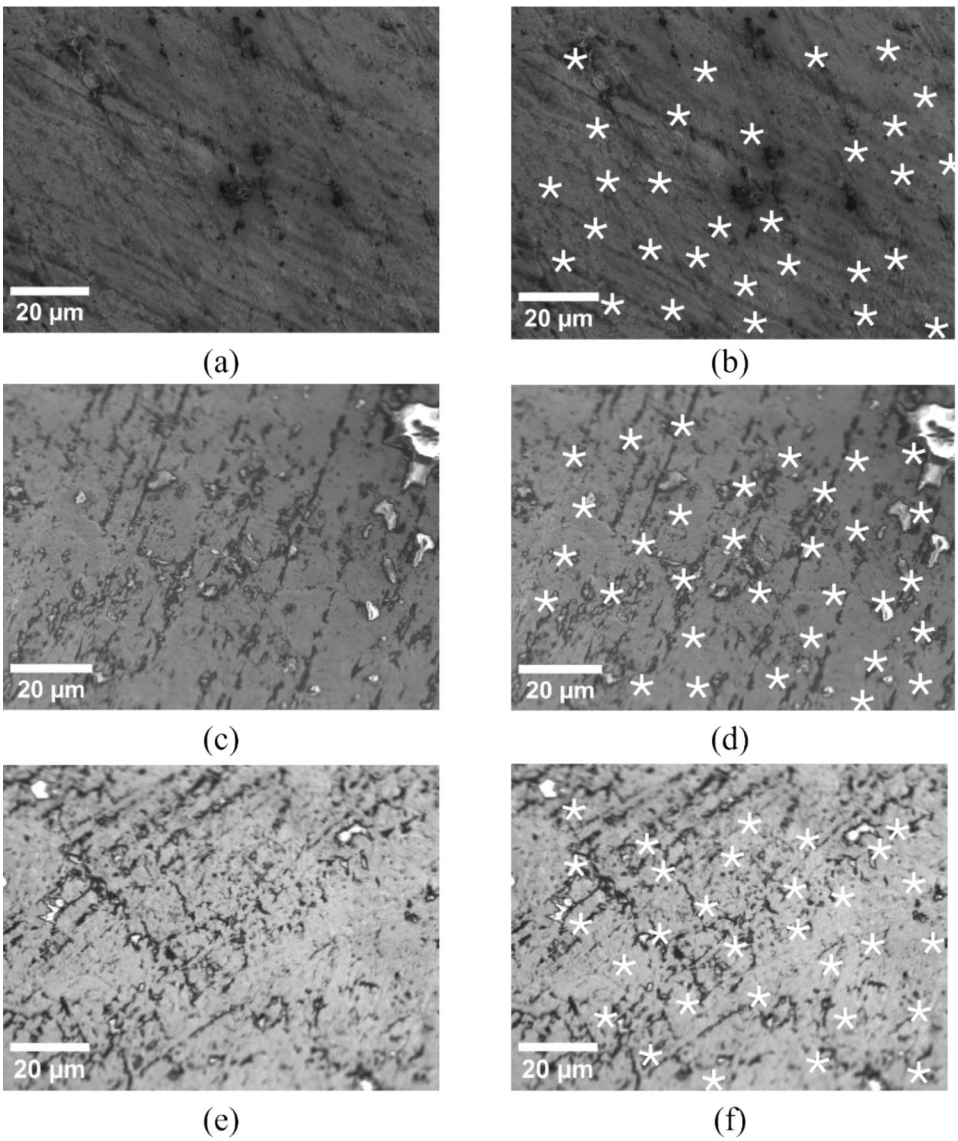

Fig. 2 SEM images of filaments prepared using different mixing methods: (**a**) DSM, (**c**) MS, and (**e**) WSM. Corresponding 30-point markings for EDS analysis are shown in(**b**),(**d**), and(**f**)

3 Results

3.1 Micro-indentation

3.1.1 Indentation hardness and elastic modulus

The hardness and elastic modulus determined from the micro-indentation are exhibited in Fig. 3a. DSM samples showed the highest hardness followed by MS and WSM samples. DSM samples also exhibited the highest elastic modulus (contact elasticity). In fact, ANOVA tests showed that the mixing method ($p < 0.0001$) significantly affected the hardness and elastic modulus of FFF-printed PLA-HA. For more details on ANOVA analysis, readers are referred to the authors' previous work [72] as well as to the comprehensive introduction to ANOVA analysis found in Reference [75]. According to the data, DSM was found to be the optimum mixing method for producing PLA-HA, if the highest hardness and elastic modulus are sought.

3.1.2 Indentation creep

Figure 3b illustrates the impact of each mixing method on indentation creep displacement under contact load holding conditions for each mixing method. ANOVA tests showed that the mixing method ($p < 0.0001$) also significantly affected the contact creep of FFF-printed PLA-HA. Similar to elastic modulus and hardness results, Fig. 3b shows that DSM is the best mixing method among all three techniques for producing PLA-HA with high creep resistance.

3.2 Elemental analysis

The two most unique constituents of HA are phosphorous (P) and calcium (Ca) which are not found in the PLA polymer matrix. Figure 4 depicts the sum spectrum obtained from the EDS analysis of the samples made through different mixing methods. EDS spectra show the presence of phosphorous (P) and calcium (Ca) on the samples which confirms the existence and integration of HA into the polymer matrix for all the methods.

3.3 Compression testing

The detailed compressive stress–strain curves from the compression testing are depicted in Fig. 5. Figure 6 compares the calculated elastic modulus whereas Fig. 7 illustrates compressive yield strength, $MACS_{50\%}$ along with the calculated modulus of resilience and $APE_{50\%}$.

DSM exhibited the highest compressive yield strength and $MACS_{50\%}$, followed by WSM and MS. Furthermore, DSM exhibited the highest moduli of elasticity and resilience and $APE_{50\%}$, followed by WSM and MS.

3.4 Post-compression SEM analysis

SEM images after compression testing were taken to analyze the failure topography. The SEM images were taken from the top side of the sample (see Fig. 8). SEM images of DSM and WSM samples are shown in Figs. 9 and 10, respectively. Due to extensive damage sustained during the compression test, it was not possible to obtain SEM images of the MS sample. Figure 9a illustrates the surface of a DSM sample after compression testing. White arrows highlight the visible surface cracks

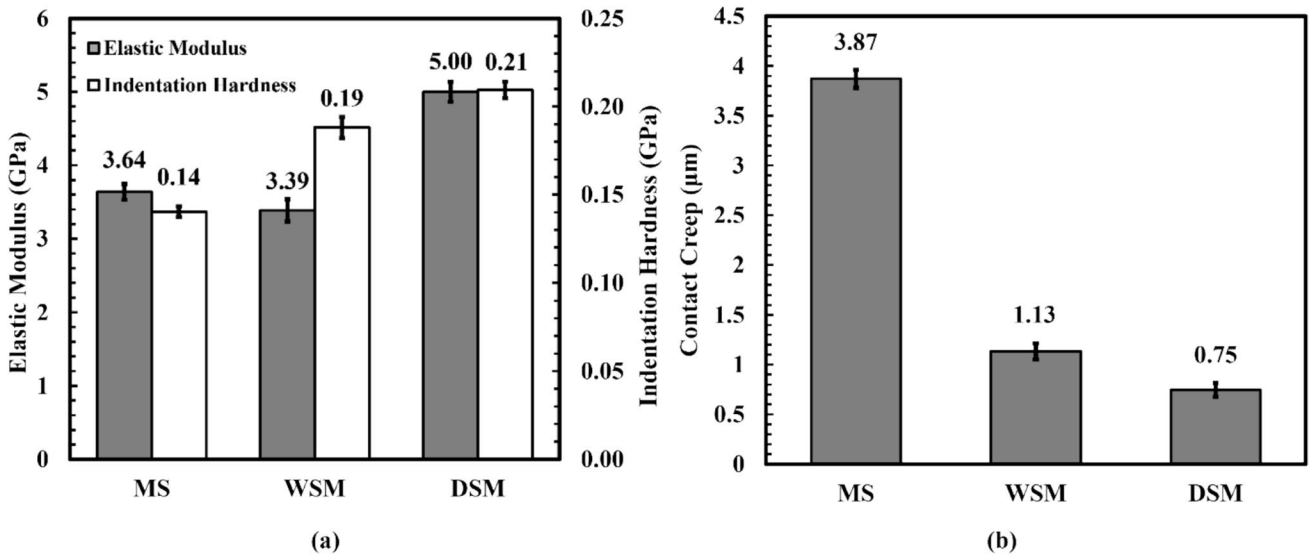

Fig. 3 Micro-indentation results: (**a**) elastic modulus and indentation hardness and (**b**) contact creep

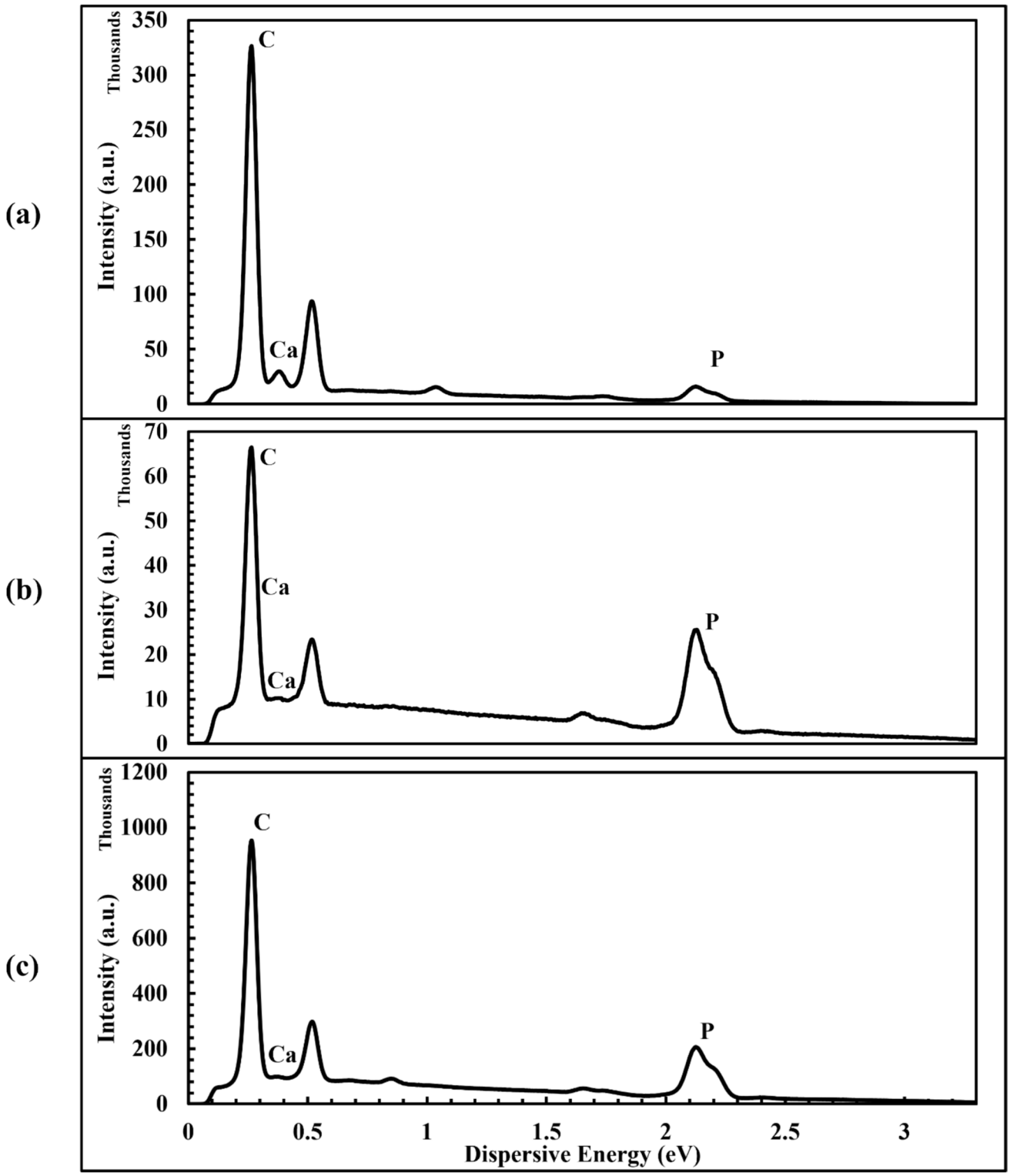

Fig. 4 EDS sum spectra of (**a**) MS, (**b**) WSM, and (**c**) DSM

and buckling that occurred on individual layers of the composite. For a closer look at one of these cracks, Fig. 9c provides a magnified view of a representative area from Fig. 9a. From Fig. 10, it is evident that the WSM sample's post-compression microstructure exhibited significantly more cracks, tears, surface cracks, and delamination. DSM microstructure (Fig. 9)

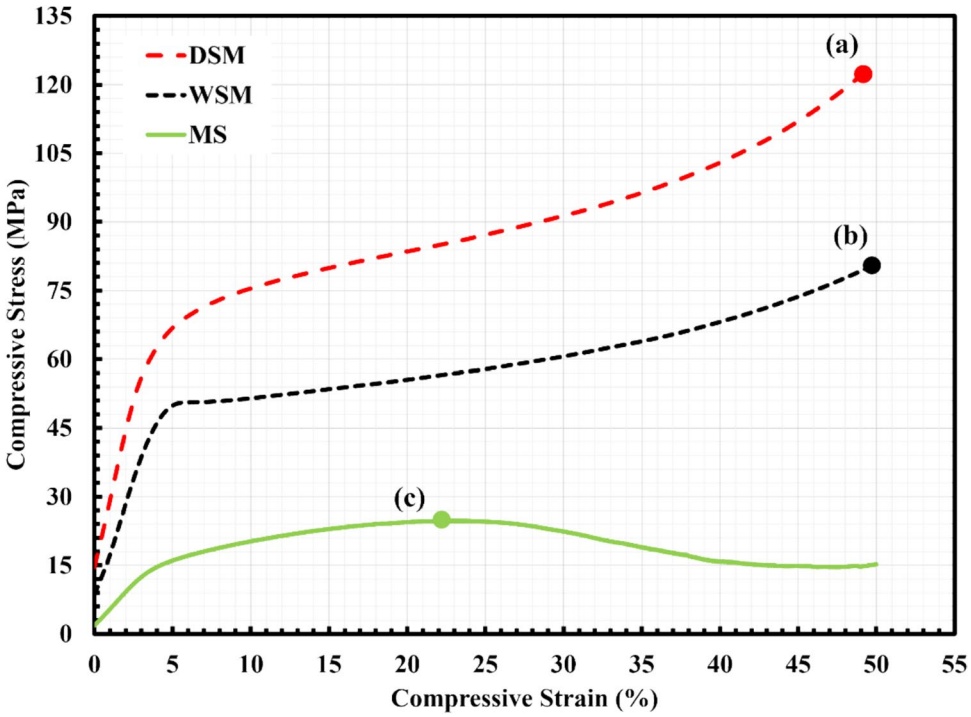

Fig. 5 Compressive stress–strain curve until 50% strain. The points labeled (**a**), (**b**), and (**c**) correspond to the $MACS_{50\%}$ for DSM, WSM, and MS samples, respectively

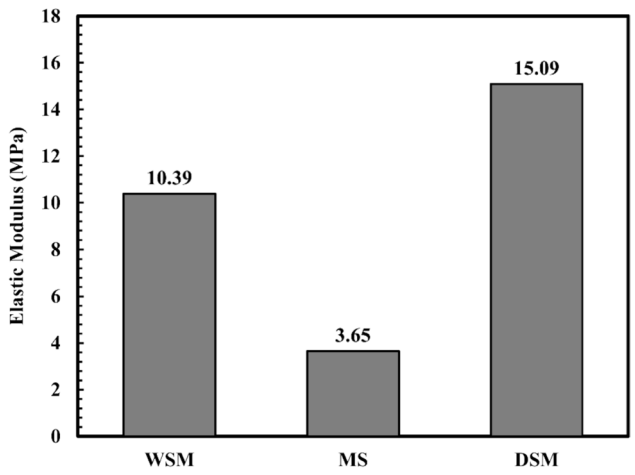

Fig. 6 Calculated elastic modulus from compression tests

remained largely intact, with minimal buckling and only a few small tears and surface cracks. These observations correlate with the superior mechanical and surface properties measured in this study for DSM samples showing the formation of different microstructures during different fabrication processes.

4 Discussion

4.1 Hardness and elastic modulus (from micro-indentation)

The statistical significance from ANOVA analysis indicated a strong influence of the mixing method ($p < 0.0001$) on the mechanical properties of FFF-printed PLA-HA composite. The data shows that DSM samples exhibited the highest indentation hardness and elastic modulus, as 0.21 ± 0.1 GPa and 5.0 ± 0.2 GPa, respectively (Fig. 3a, b). Results of elastic modulus are aligned with the values reported by Dubinenko et al. [37]. They reported that the addition of 12.5, 25, and 50 wt% HA into PLA polymer matrix led to the elastic modulus of 4774 ± 848, 6138 ± 309, and 8111 ± 714 MPa, respectively. The higher performance of the DSM mixing method likely stems from the enhanced distribution of HA particles. In fact, enhanced distribution of HA particles in the matrix has been reported for the DSM method. For example, Corcione et al. [39] noted that the filaments prepared by DSM exhibited "good dispersion of HA," and their 3D-printed PLA-HA structures demonstrated appropriate printing quality with high accuracy. They reported that this enhanced homogeneity translated to more even stress distribution and minimized weak points, ultimately leading to the higher hardness and elastic modulus observed in DSM samples. Additionally, post-compression SEM imaging of DSM samples (Fig. 9) revealed fewer micro-cracks and reduced buckling which further supports the enhanced homogeneity of HA distribution within these samples, observed in

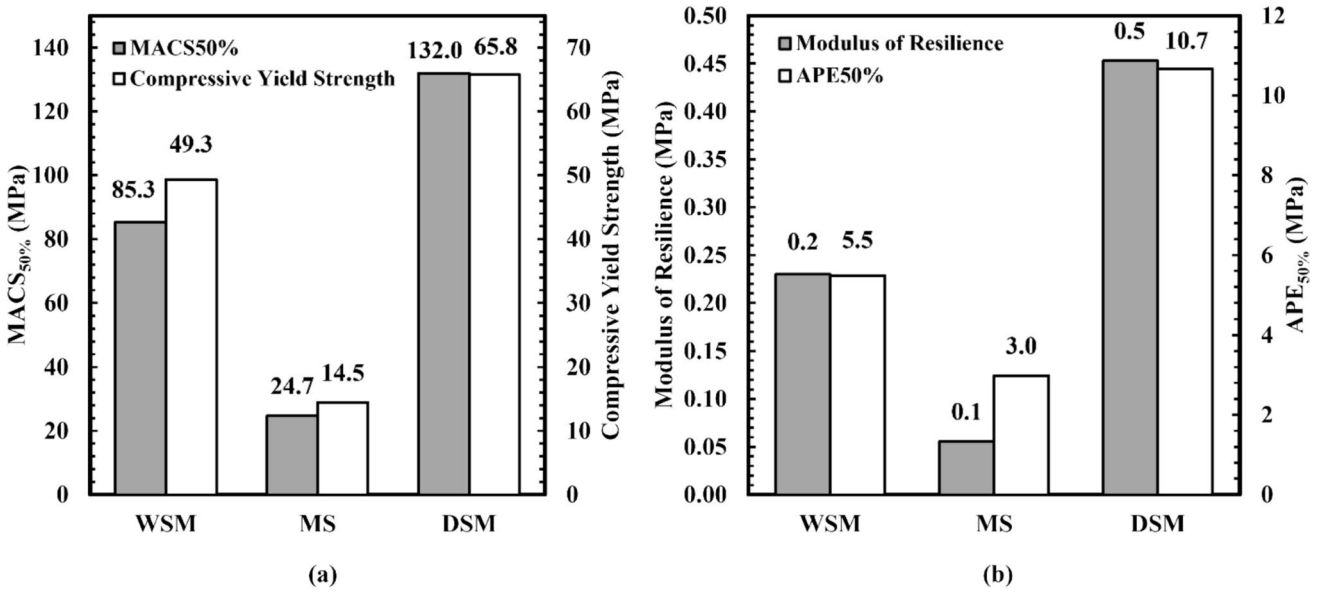

Fig. 7 (**a**) $MACS_{50\%}$ and compressive yield strength and (**b**) calculated modulus of resilience and $APE_{50\%}$

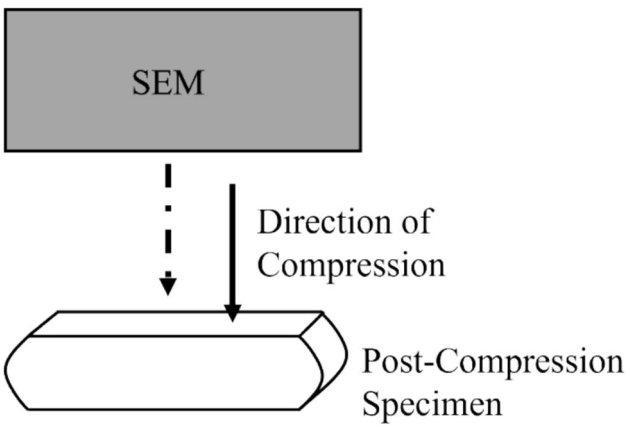

Fig. 8 Schematic of direction of SEM

this study. This enhanced HA particle distribution resulted in a stronger and more resilient material, ultimately leading to improved mechanical properties in the final printed composite.

On the other hand, PLA-HA composites prepared via MS exhibited the lowest hardness and elastic modulus. This could be attributed to two key limitations of MS compared to speed mixers. Firstly, the MS mixing method generates significantly lower shear forces, hindering the proper breakdown and distribution of HA particles throughout the PLA matrix. Secondly, MS provides a less turbulent mixing environment compared to speed mixers. This reduces the frequency of collisions between PLA and HA particles, reducing their interaction and deterring overall molecular distribution. Consequently, these weak points within the FFF-printed composite contributed to inferior mechanical performance. Indeed, these results aligned with a study by Russias et al. [42], who reported substantial HA agglomeration in PLA-HA samples prepared via MS, as well as the results of the compression test, where the MS sample was completely destroyed post-compression. Similarly, the results for the WSM samples were consistent with the study conducted by Zhang et al. [43], where they observed agglomeration of HA particles in WSM samples, leading to inferior mechanical performance. This is also evident in the SEM images of the WSM sample in Fig. 10, where significant cracks and buckling are observed.

4.2 Creep (from micro-indentation)

From the ANOVA analysis, it was observed that the mixing method ($p < 0.0001$) had a significant influence on the contact creep of FFF-printed PLA-HA. The trend in data shows that DSM exhibited the lowest contact creep of 0.75 µm, hence exhibiting the highest performance (Fig. 3b). This is correlated with a study from Han-bo et al. [76] which found that creep life decreases with increasing stress and the creep rate increases. The observed higher creep resistance in DSM samples can be attributed to stronger interfacial bonding between PLA and HA particles on the surface, likely due to the higher presence of HA detected in DSM samples compared to MS and WSM. This suggests that the enhanced dispersion of HA elements achieved through the DSM process contributed to stronger interfacial interactions (Fig. 9). In contrast, MS and WSM samples exhibited higher creep deformation, potentially due to the less presence of HA particles, which created weaker structure (Fig. 10).

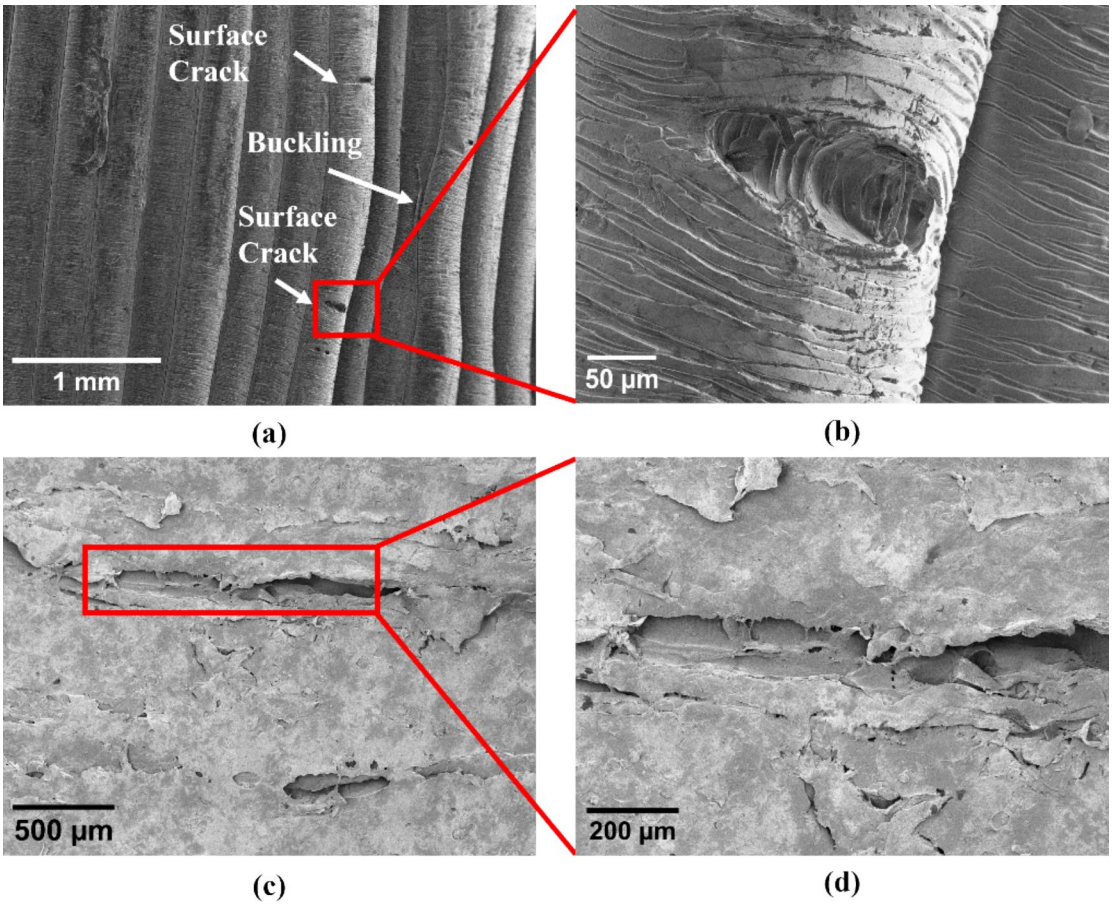

Fig. 9 SEM images of DSM sample (**a**) post-compression tears and buckling, (**b**) close-up image of tear observed in (**a**), (**c**) surface crack observed, and (**d**) close-up image of crack in (**c**)

4.3 EDS

The EDS analysis confirmed the successful integration of PLA and HA within all three composite filaments. When calculating the average P/C ratio from the 30-point EDS analysis, the standard deviation within the DSM samples (0.17) was found to be significantly lower compared to WSM (0.62) and MS (0.55) samples. These findings align with Corcione et al. [39], suggesting a more consistent distribution of HA particles within the DSM mixing method. It is also important to acknowledge that assessing homogeneity based on the P/C ratio alone may not necessarily confirm a fully homogeneous dispersion, due to the limitations in spatial resolution inherent in EDS analysis. However, in this study, the consistency suggested by the P/C ratio is corroborated by additional SEM observations. Specifically, the post-compression SEM imaging of DSM samples (Fig. 9) revealed fewer micro-cracks and reduced buckling, further supporting the interpretation of a more consistent HA particle distribution within the DSM filaments. Since the MS and WSM samples exhibited a higher standard deviation of the P/C ratio compared to the DSM samples, this could be interpreted as indicating a less consistent HA particle distribution. This inconsistency in HA dispersion is reflected in the mechanical performance of these samples as well as in the SEM images of the WSM sample (Fig. 10), which shows significant micro-cracking and tearing. These findings likely contributed to the inferior mechanical performance observed in the MS and WSM samples. Furthermore, Wang et al. [77] also observed a reduction in P weight percent in WSM composites due to encapsulation of HA particles by PLA, suggesting that the WSM process may not effectively disperse HA particles within the PLA matrix, thus leading to inferior mechanical properties. While the P/C ratio alone does not fully establish a homogeneous dispersion of HA, the consistency of these findings with SEM imaging supports that the DSM process enhances the uniformity of HA distribution, ultimately contributing to higher mechanical properties in comparison to MS and WSM samples. Future studies may employ transmission electron microscopy (TEM) on sample lamellae to gain more detailed insights into the nanoscale distribution of HA particles.

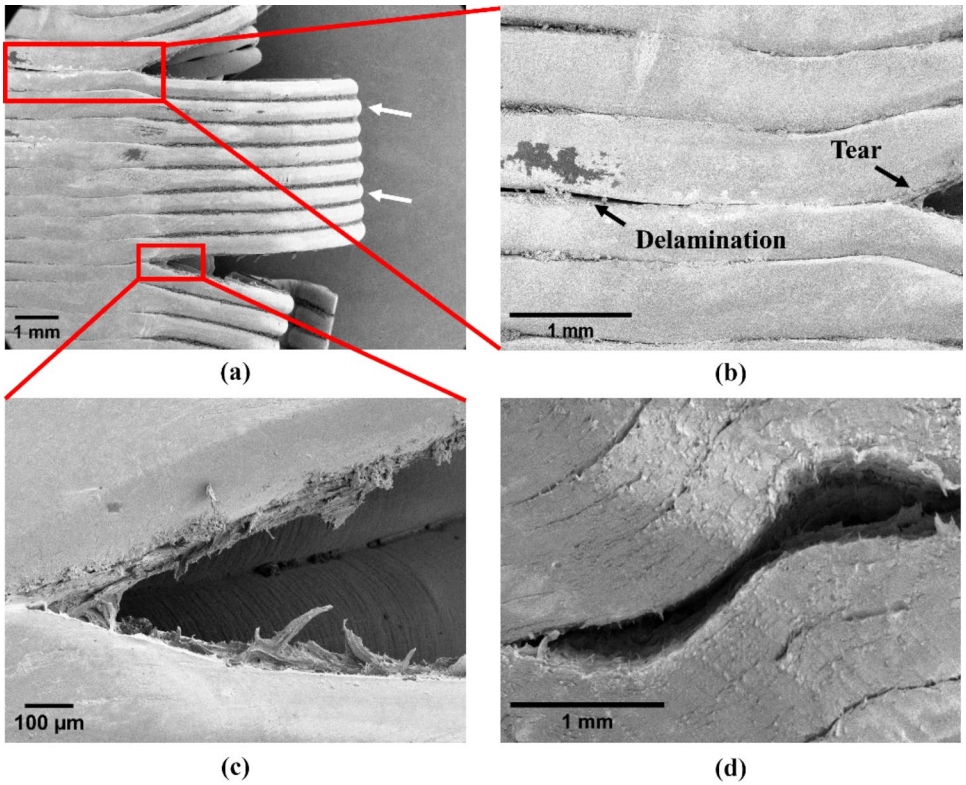

Fig. 10 SEM images of WSM sample (**a**) individual layers (white arrows) along with tears, (**b**) post-compression tear and delamination of layer, (**c**) close-up image of (**b**), and (**d**) surface crack

4.4 Compression tests

The results indicated that the selection of the mixing method significantly influenced the compressive properties of FFF-printed PLA-HA composites. DSM yielded composites with the highest compressive strength, modulus of elasticity, modulus of resilience, and $APE_{50\%}$, as illustrated in Figs. 5 and 6. This aligns also with the trends observed in micro-indentation results. The elastic modulus values obtained from compression testing and micro-indentation differ significantly due to the nature of each testing method, especially in view of the fact that we are, firstly, evaluating a composite with spatially different mechanical properties at micron-levels due to rather random dispersion of powders in the main matrix and, secondly, in general, micro-indentation here assessed surface properties with a shallow indentation depth up to 11.1 µm, reflecting the elastic modulus of only one to two surface layers [72]. On the other hand, compression tests evaluated the bulk properties of the material, encompassing all layers of the sample and the overall collective behavior of the HA particles and the main polymer matrix. In fact, these tests involved compressing the sample to a 50% strain, where the interactions between individual layers and their bonding play a crucial role in determining the bulk compressive properties. Nevertheless, results of elastic modulus are correlated with the values reported by Niaza et al. [37], where the mean value of elastic modulus was reported as 4.0 ± 0.2 GPa for PLA-nHA.

As illustrated in Fig. 9, DSM samples demonstrated superior structural integrity, characterized by fewer micro-cracks and buckling. Therefore, DSM samples outperformed MS and WSM in terms of compressive strength and hence, the moduli of elasticity and resilience, and $APE_{50\%}$. As depicted in Fig. 9, more extensive micro-cracking and tearing were observed in SEM imaging of WSM samples, leading to an earlier failure as compared to its DSM counterpart. The post-compression sample of the MS sample was destroyed, making it impossible to obtain SEM images. These observations underscore the critical role of mixing methods in determining the mechanical properties of PLA-HA composites such as PLA-HA and validate the effectiveness of the DSM process in enhancing mechanical performance.

5 Conclusion

In this study, a comparative analysis approach was utilized to evaluate the significance of three distinct mixing methods—MS, WSM, and DSM—on the surface and mechanical properties of FFF-printed PLA-HA composites. Micro-indentation tests demonstrated that DSM yielded the highest elastic modulus, hardness, and the lowest creep resistance, outperforming both MS and WSM samples. Compressive testing corroborated these findings, with DSM composites exhibiting superior moduli of elasticity and resilience, $APE_{50\%}$, and $MACS_{50\%}$ compared to MS and WSM counterparts. SEM

analysis supported these observations by showing minor cracks and little buckling on the surface of DSM composites. EDS confirmed the presence of HA particles in all three composite filaments. It is suggested that more uniform dispersion of HA particles with PLA matrix can be achieved through DSM technique. This could be the main reason for improved mechanical properties, establishing DSM as the optimum mixing method. This study highlighted the synergistic relationship between FFF printing technology and mixing methods. The findings from this research will contribute valuable insights to the broader field of FFF printing and polymer composite formulation. Moving forward, future research efforts can focus on further refining the DSM process parameters to potentially achieve even better dispersion. Additionally, exploring the impact of other factors, such as final printing parameters and post-processing techniques, on the surface and mechanical properties of FFF-printed polymer composites holds promise for further optimization.

Acknowledgements The author would like to thank Mr. Shaheen Mahmood for help with conducting the indentation tests, Dr. Leila Sabri for assistance with the EDS tutorial, and Mr. Johnnie Hall, IV for help with 3D printing the samples.

Author contribution All authors contributed to the study conception and design. Sample design and preparation were performed by Alexander Stuart and Violetta Rostobaya; data collection and analysis were performed by Muhammad Zaryyab Sardar, Kunal Manoj Gide, and Kian Zarrabinia. The first draft of the manuscript was written by Muhammad Zaryyab Sardar, edited, and revised. The manuscript was reviewed by Kunal Manoj Gide, Ali Beheshti, and Shaghayegh Bagheri. All authors read and approved the final manuscript.

Funding This work was supported by George Mason University's Undergraduate Research Scholars Program (URSP) [Grant Number: 160749, Activity Code: URSP2S].

Data availability All data is included in the paper.

Declarations

Conflict of interest The authors declare no competing interests.

References

1. Huang Y, Leu MC, Mazumder J, Donmez A (2015) Additive manufacturing: current state, future potential, gaps and needs, and recommendations. J Manuf Sci Eng 137(1):014001. https://doi.org/10.1115/1.4028725
2. Saleh Alghamdi S, John S, Roy Choudhury N, Dutta NK (2021) Additive manufacturing of polymer materials: progress, promise and challenges. Polymers 13:753. https://doi.org/10.3390/polym13050753
3. Tofail SAM, Koumoulos EP, Bandyopadhyay A et al (2018) Additive manufacturing: scientific and technological challenges, market uptake and opportunities. Mater Today 21:22–37. https://doi.org/10.1016/j.mattod.2017.07.001
4. Mobarak MH, Islam MdA, Hossain N et al (2023) Recent advances of additive manufacturing in implant fabrication – a review. Appl Surf Sci Adv 18:100462. https://doi.org/10.1016/j.apsadv.2023.100462
5. Bi J, Liu Z, Li B et al (2024) Additive manufacturing of thermoelectric materials: materials, synthesis and manufacturing: a review. J Mater Sci 59:359–381. https://doi.org/10.1007/s10853-023-08953-y
6. Zhou L, Miller J, Vezza J et al (2024) Additive manufacturing: a comprehensive review. Sensors 24:2668. https://doi.org/10.3390/s24092668
7. Lynn R, Dinar M, Huang N et al (2017) Direct digital subtractive manufacturing of a functional assembly using voxel-based models. J Manuf Sci Eng 140:021006. https://doi.org/10.1115/1.4037631
8. Rashid AB, Haque M, Islam SMM, Uddin Labib KMR (2024) Nanotechnology-enhanced fiber-reinforced polymer composites: recent advancements on processing techniques and applications. Heliyon 10:e24692. https://doi.org/10.1016/j.heliyon.2024.e24692
9. Fico D, Rizzo D, Casciaro R, Esposito Corcione C (2022) A review of polymer-based materials for fused filament fabrication (FFF): focus on sustainability and recycled materials. Polymers 14:465. https://doi.org/10.3390/polym14030465
10. Rao CH, Avinash K, Varaprasad BKSVL, Goel S (2022) A review on printed electronics with digital 3D printing: fabrication techniques, materials, challenges and future opportunities. J Electron Mater 51:2747–2765. https://doi.org/10.1007/s11664-022-09579-7
11 Prashar G, Vasudev H, Bhuddhi D (2022) Additive manufacturing: expanding 3D printing horizon in Industry 4.0. Int J Interact Des Manuf IJIDeM 17(5):2221–2235. https://doi.org/10.1007/s12008-022-00956-4
12. Altıparmak SC, Yardley VA, Shi Z, Lin J (2022) Extrusion-based additive manufacturing technologies: state of the art and future perspectives. J Manuf Process 83:607–636. https://doi.org/10.1016/j.jmapro.2022.09.032
13. Litke Q, Wahbi M, Kontopoulou M et al (2023) Epoxidized canola oil as an environmentally friendly compatibilizer for blending poly(lactic acid) and poly(butylene adipate-co-terephthalate). J Mater Sci 58:17691–17710. https://doi.org/10.1007/s10853-023-09141-8
14. Ghassemi B, Estaji S, Mousavi SR et al (2022) In-depth study of mechanical properties of poly(lactic acid)/thermoplastic polyurethane/hydroxyapatite blend nanocomposites. J Mater Sci 57:7250–7264. https://doi.org/10.1007/s10853-022-07129-4
15. Aliotta L, Dal Pont B, Gigante V et al (2024) Investigation of new poly(lactic acid) (PLA)/poly(butylene succinate-co-adipate) (PBSA) thermoplastic composites reinforced with different amount of twill hemp fabrics. J Mater Sci 59:847–862. https://doi.org/10.1007/s10853-023-09231-7

16. Pérez E (2021) Mechanical performance of in vitro degraded polylactic acid/hydroxyapatite composites. J Mater Sci 56:19915–19935. https://doi.org/10.1007/s10853-021-06508-7
17. Tümer EH, Erbil HY (2021) Extrusion-based 3D printing applications of PLA composites: a review. Coatings 11:390. https://doi.org/10.3390/coatings11040390
18. Wickramasinghe S, Do T, Tran P (2020) FDM-based 3D printing of polymer and associated composite: a review on mechanical properties, defects and treatments. Polymers 12:1529. https://doi.org/10.3390/polym12071529
19. Baran EH, Erbil HY (2019) Surface modification of 3D printed PLA objects by fused deposition modeling: a review. Colloids Interfaces 3:43. https://doi.org/10.3390/colloids3020043
20. Mazzanti V, Malagutti L, Mollica F (2019) FDM 3D printing of polymers containing natural fillers: a review of their mechanical properties. Polymers 11:1094. https://doi.org/10.3390/polym11071094
21. Subramaniam SR, Samykano M, Selvamani SK et al (2019) 3D printing: overview of PLA progress. AIP Conf Proc 2059:020015. https://doi.org/10.1063/1.5085958
22. Chen X, Chen G, Wang G et al (2020) Recent progress on 3D-printed polylactic acid and its applications in bone repair. Adv Eng Mater 22:1901065. https://doi.org/10.1002/adem.201901065
23. Bourang S, Asadian S, Noruzpour M et al (2024) PLA-HA/Fe3O4 magnetic nanoparticles loaded with curcumin: physicochemical characterization and toxicity evaluation in HCT116 colorectal cancer cells. Discov Appl Sci 6:186. https://doi.org/10.1007/s42452-024-05858-6
24. Thakur VK, Singha AS, Thakur MK (2012) Biopolymers based green composites: mechanical, thermal and physico-chemical characterization. J Polym Environ 20:412–421. https://doi.org/10.1007/s10924-011-0389-y
25. Farah S, Anderson DG, Langer R (2016) Physical and mechanical properties of PLA, and their functions in widespread applications — a comprehensive review. Adv Drug Deliv Rev 107:367–392. https://doi.org/10.1016/j.addr.2016.06.012
26. Chacón JM, Caminero MA, García-Plaza E, Núñez PJ (2017) Additive manufacturing of PLA structures using fused deposition modelling: effect of process parameters on mechanical properties and their optimal selection. Mater Des 124:143–157. https://doi.org/10.1016/j.matdes.2017.03.065
27. Zaaba NF, Jaafar M (2020) A review on degradation mechanisms of polylactic acid: hydrolytic, photodegradative, microbial, and enzymatic degradation. Polym Eng Sci 60:2061–2075. https://doi.org/10.1002/pen.25511
28. Ielo I, Calabrese G, De Luca G, Conoci S (2022) Recent advances in hydroxyapatite-based biocomposites for bone tissue regeneration in orthopedics. Int J Mol Sci 23:9721. https://doi.org/10.3390/ijms23179721
29. Shi H, Zhou Z, Li W et al (2021) Hydroxyapatite based materials for bone tissue engineering: a brief and comprehensive introduction. Crystals 11:149. https://doi.org/10.3390/cryst11020149
30. Xiao L, Wang B, Yang G et al (2012) Poly(lactic acid)-based biomaterials: synthesis, modification and applications. In: Biomedical Science, Engineering and Technology. IntechOpen, pp 247–248. https://doi.org/10.5772/23927
31. Meyhami T, Hassanajili S, Tanideh N, Taheri E (2024) Three dimensional scaffolds of hybrid PLA/PCL/HA/silica nanocomposites for bone tissue engineering. Polym Bull 81:6025–6053. https://doi.org/10.1007/s00289-023-04978-0
32. Joseph TM, Kallingal A, Suresh AM et al (2023) 3D printing of polylactic acid: recent advances and opportunities. Int J Adv Manuf Technol 125:1015–1035. https://doi.org/10.1007/s00170-022-10795-y
33. Balla E, Daniilidis V, Karlioti G et al (2021) Poly(lactic acid): a versatile biobased polymer for the future with multifunctional properties—from monomer synthesis, polymerization techniques and molecular weight increase to PLA applications. Polymers 13:1822. https://doi.org/10.3390/polym13111822
34. Z. Naser A, Deiab I, M. Darras B, (2021) Poly(lactic acid) (PLA) and polyhydroxyalkanoates (PHAs), green alternatives to petroleum-based plastics: a review. RSC Adv 11:17151–17196. https://doi.org/10.1039/D1RA02390J
35. Damadzadeh B, Jabari H, Skrifvars M et al (2010) Effect of ceramic filler content on the mechanical and thermal behaviour of poly-L-lactic acid and poly-L-lactic-co-glycolic acid composites for medical applications. J Mater Sci Mater Med 21:2523–2531. https://doi.org/10.1007/s10856-010-4110-9
36. Kędzierska-Matysek M, Matwijczuk A, Florek M et al (2018) Application of FTIR spectroscopy for analysis of the quality of honey. BIO Web Conf 10:02008. https://doi.org/10.1051/bioconf/20181002008
37. Niaza KV, Senatov FS, Kaloshkin SD et al (2016) 3D-printed scaffolds based on PLA/HA nanocomposites for trabecular bone reconstruction. J Phys Conf Ser 741:012068. https://doi.org/10.1088/1742-6596/741/1/012068
38. Solechan S, Suprihanto A, Widyanto SA et al (2023) Characterization of PLA/PCL/nano-hydroxyapatite (nHA) biocomposites prepared via cold isostatic pressing. Polymers 15:559. https://doi.org/10.3390/polym15030559
39. Corcione CE, Gervaso F, Scalera F et al (2017) 3D printing of hydroxyapatite polymer-based composites for bone tissue engineering. J Polym Eng 37:741–746. https://doi.org/10.1515/polyeng-2016-0194
40. Gide KM, Islam S, Bagheri ZS (2022) Polymer-based materials built with additive manufacturing methods for orthopedic applications: a review. J Compos Sci 6:262. https://doi.org/10.3390/jcs6090262
41. Ferri J, Jordá J, Montanes N et al (2018) Manufacturing and characterization of poly(lactic acid) composites with hydroxyapatite. J Thermoplast Compos Mater 31:865–881. https://doi.org/10.1177/0892705717729014
42. Russias J, Saiz E, Nalla RK et al (2006) Fabrication and mechanical properties of PLA/HA composites: a study of in vitro degradation. Mater Sci Eng C Biomim Supramol Syst 26:1289–1295. https://doi.org/10.1016/j.msec.2005.08.004
43. Zhang B, Wang L, Song P et al (2021) 3D printed bone tissue regenerative PLA/HA scaffolds with comprehensive performance optimizations. Mater Des 201:109490. https://doi.org/10.1016/j.matdes.2021.109490
44. Cardoso GBC, Ramos SLF, Rodas ACD et al (2010) Scaffolds of poly (ε-caprolactone) with whiskers of hydroxyapatite. J Mater Sci 45:4990–4993. https://doi.org/10.1007/s10853-010-4363-1
45. Doyle SE, Henry L, McGennisken E et al (2021) Characterization of polycaprolactone nanohydroxyapatite composites with tunable degradability suitable for indirect printing. Polymers 13:295. https://doi.org/10.3390/polym13020295
46. Ke K, Wang Y, Liu X-Q et al (2012) A comparison of melt and solution mixing on the dispersion of carbon nanotubes in a poly(vinylidene fluoride) matrix. Compos Part B Eng 43:1425–1432. https://doi.org/10.1016/j.compositesb.2011.09.007
47. Arora N, Dua S, Singh VK et al (2024) A comprehensive review on fillers and mechanical properties of 3D printed polymer composites. Mater Today Commun 40:109617. https://doi.org/10.1016/j.mtcomm.2024.109617
48. Guan L-Z, Tang L-C (2020) Dispersion and alignment of carbon nanotubes in polymer matrix. In: Abraham J, Thomas S, Kalarikkal N (eds) Handbook of Carbon Nanotubes. Springer International Publishing, Cham, pp 1–35

49. Ali Z, Yaqoob S, Yu J, D'Amore A (2024) Unveiling the influential factors and heavy industrial applications of graphene hybrid polymer composites. J Compos Sci 8:183. https://doi.org/10.3390/jcs8050183
50. Esawi A, Salem H, Hussein H, Ramadan A (2009) Effect of processing technique on the dispersion of carbon nanotubes within polypropylene carbon nanotube-composites and its effect on their mechanical properties. Polym Compos 31:772–780. https://doi.org/10.1002/pc.20859
51. Guchait A, Saxena A, Chattopadhyay S, Mondal T (2022) Influence of nanofillers on adhesion properties of polymeric composites. ACS Omega 7:3844–3859. https://doi.org/10.1021/acsomega.1c05448
52. Pattanayak I, Alex Y, Mohanty S (2023) Advancing strategies towards the development of tissue engineering scaffolds: a review. J Mater Sci 58:12847–12898. https://doi.org/10.1007/s10853-023-08798-5
53. Wu D, Spanou A, Diez-Escudero A, Persson C (2020) 3D-printed PLA/HA composite structures as synthetic trabecular bone: a feasibility study using fused deposition modeling. J Mech Behav Biomed Mater 103:103608. https://doi.org/10.1016/j.jmbbm.2019.103608
54. DeStefano V, Khan S, Tabada A (2020) Applications of PLA in modern medicine. Eng Regen 1:76–87. https://doi.org/10.1016/j.engreg.2020.08.002
55. Wang W, Zhang B, Zhao L et al (2021) Fabrication and properties of PLA/nano-HA composite scaffolds with balanced mechanical properties and biological functions for bone tissue engineering application. Nanotechnol Rev 10:1359–1373. https://doi.org/10.1515/ntrev-2021-0083
56. Banpean A, Hararak B, Winotapun C et al (2023) Lignin nanoparticles as sustainable biobased nucleating agents of poly(L-lactic acid): crystallization behavior and effect of particle sizes. J Mater Sci 58:6823–6838. https://doi.org/10.1007/s10853-023-08418-2
57. Grigora M-E, Terzopoulou Z, Baciu D et al (2023) 3D printed poly(lactic acid)-based nanocomposite scaffolds with bioactive coatings for tissue engineering applications. J Mater Sci 58:2740–2763. https://doi.org/10.1007/s10853-023-08149-4
58. Duan X, Li Y, Song D et al (2023) Eco-friendly porous poly(lactic acid)/alkali-treated walnut shell powder composites for the removal of methylene blue. J Mater Sci 58:18073–18089. https://doi.org/10.1007/s10853-023-09210-y
59. Zeng S, Hou Y, Zhou Y et al (2022) Adsorptive removal of uremic toxins using Zr-based MOFs for potential hemodialysis membranes. J Mater Sci 57:2909–2923. https://doi.org/10.1007/s10853-021-06783-4
60. Eryildiz M (2024) Tailoring mechanical properties of FDM-3D-printed parts through titanium dioxide-reinforced resin filling technique. Proc Inst Mech Eng Part B J Eng Manuf 09544054241260467. https://doi.org/10.1177/09544054241260467
61. Tuli NT, Khatun S, Rashid AB (2024) Unlocking the future of precision manufacturing: a comprehensive exploration of 3D printing with fiber-reinforced composites in aerospace, automotive, medical, and consumer industries. Heliyon 10:e27328. https://doi.org/10.1016/j.heliyon.2024.e27328
62. Costa JM, Sequeiros EW, Vieira MF (2023) Fused filament fabrication for metallic materials: a brief review. Materials 16:7505. https://doi.org/10.3390/ma16247505
63. Mahmood A, Perveen F, Chen S et al (2024) Polymer composites in 3D/4D printing: materials, advances, and prospects. Molecules 29:319. https://doi.org/10.3390/molecules29020319
64. Petrovskaya TS, Toropkov NE, Mironov EG, Azarmi F (2018) 3D printed biocompatible polylactide-hydroxyapatite based material for bone implants. Mater Manuf Process 33:1899–1904. https://doi.org/10.1080/10426914.2018.1476764
65. Backes EH, Pires LDN, Beatrice CAG et al (2020) Fabrication of biocompatible composites of poly(lactic acid)/hydroxyapatite envisioning medical applications. Polym Eng Sci 60:636–644. https://doi.org/10.1002/pen.25322
66. Olesik P, Kozioł M, Konik D, Jała J (2019) The use of shredded car windscreen waste as reinforcement of thermoplastic composites for 3D (FDM) printing. Compos Theory Pract 19(1):30–33
67. Wang P, Zou B, Ding S et al (2020) Preparation of short CF/GF reinforced PEEK composite filaments and their comprehensive properties evaluation for FDM-3D printing. Compos Part B Eng 198:108175. https://doi.org/10.1016/j.compositesb.2020.108175
68. Pitjamit S, Thunsiri K, Nakkiew W et al (2020) The possibility of interlocking nail fabrication from FFF 3D printing PLA/PCL/HA composites coated by local silk fibroin for canine bone fracture treatment. Materials 13:1564. https://doi.org/10.3390/ma13071564
69. Sterman S, Marsden JG (1966) The effect of silane coupling agents in improving the properties of filled or reinforced thermoplastics. Polym Eng Sci 6:97–112. https://doi.org/10.1002/pen.760060203
70. Standard test method for measuring the damage resistance of a fiber-reinforced polymer-matrix composite to a concentrated quasi-static indentation force. https://www.astm.org/d6264_d6264m-17.html. Accessed 11 May 2024
71. Palma T, Munther M, Damasus P et al (2019) Multiscale mechanical and tribological characterizations of additively manufactured polyamide 12 parts with different print orientations. J Manuf Process 40:76–83. https://doi.org/10.1016/j.jmapro.2019.03.004
72. Pulipaka A, Gide KM, Beheshti A, Bagheri ZS (2023) Effect of 3D printing process parameters on surface and mechanical properties of FFF-printed PEEK. J Manuf Process 85:368–386. https://doi.org/10.1016/j.jmapro.2022.11.057
73. Salari S, Rahman MS, Polycarpou AA, Beheshti A (2020) Elevated temperature mechanical properties of Inconel 617 surface oxide using nanoindentation. Mater Sci Eng A 788:139539. https://doi.org/10.1016/j.msea.2020.139539
74. Standard test method for compressive properties of rigid plastics. https://www.astm.org/d0695-15.html. Accessed 11 May 2024
75. Dean A, Voss D, Draguljić D (2017) Designs with one source of variation. In: Dean A, Voss D, Draguljić D (eds) Design and Analysis of Experiments. Springer International Publishing, Cham, pp 31–68
76. Han-bo Y, Ling W (2015) Study on creep behavior of PLA/HA composites. J Xihua Univ Sci Ed 34:22–26. https://doi.org/10.3969/j.issn.1673-159X.2015.01.004
77. Wang Y, Xie M, Wang X, Zhou Z (2022) Numerical calculation and properties study on polylactic acid (PLA)/nano-hydroxyapatite (n-HA) composite fluid 3D printed by fused deposition modeling. https://doi.org/10.21203/rs.3.rs-2113565/v1